RESEARCH ARTICLE | FEBRUARY 27 2023

Describing mechanical damage evolution through *in situ* electrical resistance measurements

Special Collection: Functional Coatings

David D. Gebhart ; Anna Krapf ; Benoit Merle ; Christoph Gammer ; Megan J. Cordill

Journal of Vacuum Science & Technology A 41, 023408 (2023)
https://doi.org/10.1116/6.0002362

JVST A
Journal of Vacuum Science & Technology A

ARTICLE

avs.scitation.org/journal/jva

Describing mechanical damage evolution through *in situ* electrical resistance measurements

Cite as: J. Vac. Sci. Technol. A **41**, 023408 (2023); doi: 10.1116/6.0002362
Submitted: 15 November 2022 · Accepted: 27 January 2023 ·
Published Online: 27 February 2023

David D. Gebhart,[1,a)] Anna Krapf,[2] Benoit Merle,[3] Christoph Gammer,[1] and Megan J. Cordill[1]

AFFILIATIONS

[1]Erich Schmid Institute of Materials Science, Austrian Academy of Sciences, Jahnstrasse 12 8700, Leoben, Austria
[2]Department of Materials Science & Engineering, Institute 1, University of Erlangen-Nürnberg (FAU), Martensstrasse 5, 91058 Erlangen, Germany
[3]Institute of Materials Engineering, University of Kassel, Moenchebergstr. 3, 34125 Kassel, Germany

Note: This paper is a part of the 2023 Special Topic Collection on Functional Coatings.
[a)]**Electronic mail:** david.gebhart@oeaw.ac.at

ABSTRACT

The fatigue properties of metallizations used as electrical conductors in flexible electronic devices have been thoroughly studied over the years. Most studies use time-intensive characterization methods to evaluate mechanical damage. For their ease of access, *in situ* electrical resistance measurements are often performed along with other characterization methods. However, the data are mostly used as an indicator of failure and a thorough analysis is usually missing. This work presents some deeper analysis methods of such datasets, using gold films on polyimide, with and without a chromium interlayer, revealing that grain growth, through-thickness cracking, and more general fatigue behavior can be determined from electrical resistance data alone. A case is made for increased utilization of such easily obtained data, reducing the time required for the evaluation of experiments.

I. INTRODUCTION

With the increasing demand for long-lasting flexible and form-adjusting thin film electronic devices and components, there is a need to better understand the fatigue properties of metallizations used as electric conductors. Such electrical connections often consist of a rather ductile face-centered cubic (fcc) metal film (e.g., Cu, Ag, and Au) on a polymer substrate. The work of adhesion in those systems can be low and an increase in adhesion between the substrate and metal film was shown to improve fatigue properties.[1] An intrinsic increase in adhesion is hardly achievable. Instead, a thin adhesion promoting layer (in the low nm range) is often placed between the substrate and conductive coating, where body-centered cubic (bcc) metals have been shown to fulfill the requirements well. Metals used in interlayers include Ta,[2,3] Mo,[4] and Cr.[2,5,6] Studies in the fatigue properties of such systems mainly utilize time-intensive microscopy methods to characterize the degradation processes, with inspections mostly being performed intermittently or post loading. Conventional methods have revealed several factors that influence the fatigue properties of thin film electronic conductors, such as film thickness or grain size.[7–9] While a thin 5 nm Ti interlayer was shown to improve the longevity of 1 μm Au films,[10] in systems of thinner functional layers and thicker interlayers, the interlayer can be detrimental to damage resistance.[11]

While many studies also perform *in situ* electrical resistance measurements during cyclic loading,[12–14] the recorded data are mostly used as an indicator of failure when the normalized resistance increases above a certain threshold. Since it is not easy to observe mechanical damage *in situ*, little research has so far been done to correlate specific changes in the electrical resistance data to mechanical damage evolution. Finding such correlations and the development of general methods to observe mechanical degradation in film conductors in electrical data will greatly improve the ease of studying such systems in the future. A novel method to analyze electrical data was recently introduced that uses the evolution of electrical resistance peak widths to differentiate between surface damage and through-thickness cracks (TTCs).[15]

The datasets studied in this work were obtained from material systems with and without an adhesion promoting interlayer while keeping the functional layer's thickness, grain size, and texture constant. Gold was used as the functional layer for its chemical inertness. Without the formation of an oxide layer upon contact with air, cracks that close at strain minima during cyclical loading will better recover their conductivity, enhancing the information contained in electrical resistance datasets. This work demonstrates that certain correlations can be found and that those correlations can indicate how damage propagates, microstructure changes in the film (i.e., grain growth), and what type of damage is present over the progression of a fatigue experiment.

II. MATERIALS AND METHODS

The investigated material systems consist of 150 nm Au films deposited on 50 μm thick polyimide substrates (Upilex-S obtained from Merck KGaA) with and without a 30 nm Cr interlayer. The films were produced by thermal evaporation using a custom-built deposition system described in Ref. 16 at a base pressure between 10^{-7} and 10^{-6} mbar with deposition rates of approximately 1 Å/s (Au) and between 0.5 and 0.8 Å/s (Cr). During depositions, the substrate was heated to 80 °C (Au depositions) and 150 °C (Cr). The samples were cyclically loaded with an MTS Tytron 250, applying a sinusoidal load under strain control at a frequency of 0.5 Hz. Using a gauge length of 15 mm, the maximum strain amplitude was 2% while the minimum value was set to 0.2% as minima values of 0% showed buckling of the samples due to compressive stress induced by the viscoelastic properties of the substrate. During loading, four-point resistance measurements were taken with a Keithley 2000 multimeter at a power line cycle setting of 1, resulting in approximately 20 data points per cycle. At each side, the samples were fixed with custom-built steel clamps on top, with two pins attached to the top of each clamp to connect the

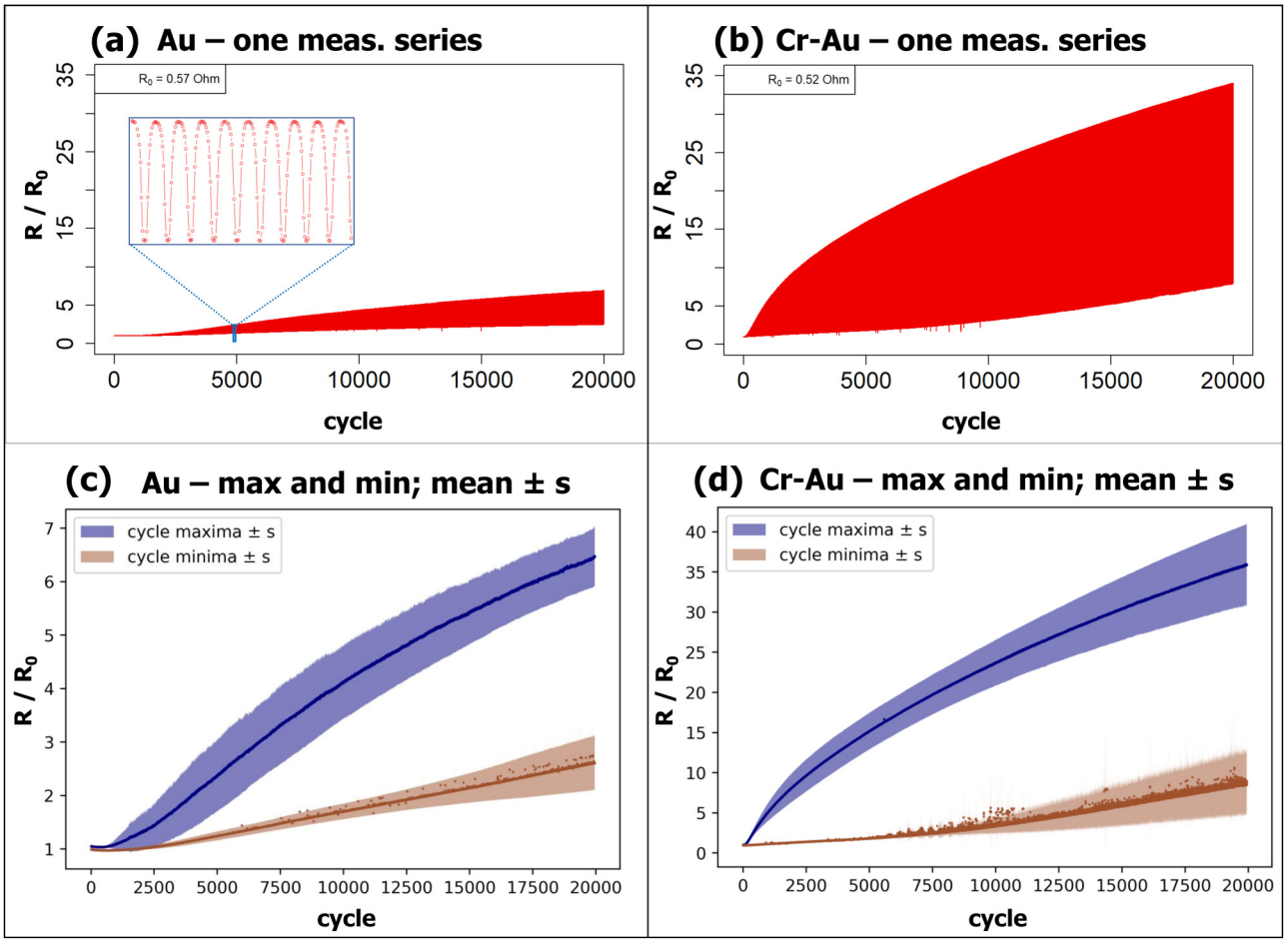

FIG. 1. Resistance data (R/R_0) of cyclically strained (2%) 150 nm Au (a) and (c) and 30 nm Cr/150 nm Au bilayer (b) and (d) on PI. In (a) and (b), all data points for one measurement series up to 20 000 cycles are shown. In (c) and (d), the averages of five measurement series are shown—cycle maxima (blue) and cycle minima (brown). The error bars are ±1 sample standard deviation. Note the different y-scale in (c) and (d).

multimeter, and polycarbonate spacers were present under the sample to ensure that there cannot be any parallel conductive pathways. The lowest range setting of the Keithley 2000 multimeter was used which utilizes a test current of 1 mA. All measured values were above 0.4 and below 25 Ω. The data were analyzed in their normalized form as a ratio of electrical resistance, R, over initial resistance, R_0. The unloaded samples were imaged by scanning electron microscopy (SEM) in a Zeiss LEO 1525 and electron backscatter diffraction (EBSD) characterization was performed using a Tescan Magna with a Bruker eflash FS detector and Bruker's ESPRIT software, using a pixel size of 25 nm. To access the Cr interlayer for characterization, the Au layer was removed in several samples with aqua regia, 5 ml HNO_3 (65%) added to 20 ml of HCl (32%), and SEM images were taken from the same regions before and after etching. Linear crack density measurements were performed by drawing nine lines of 65 μm length, parallel to the straining direction, in SEM images of different sample regions and counting the number of intersections with damage sites.

III. RESULTS AND DISCUSSION

First, a look at complete electrical resistance datasets acquired within this study reveals some general trends. Figures 1(a) and 1(b) show plots of one dataset of all acquired data points for both, the single layer (Au) and double layer (Cr–Au) systems, with an inset of 10 cycles for the Au sample. Figures 1(c) and 1(d) show only the maxima and the minima data points for each cycle, taken from five measurement series and plotted as mean ± one sample standard deviation(s), revealing good reproducibility of the measurements. The maxima data points contain information about damage initiation and propagation while the minima data points mirror crack closure properties and damage recovery at minima strain values. It can be seen that maxima values follow the general trend of an increasing slope at the beginning, a region of maximum slope, and an onset of saturation where the slope starts to decrease again. The change in slope is better visualized in Fig. 2 where only the first 2500 cycles are plotted for the Cr–Au system because the transitions occur at earlier cycle numbers than in the single layer Au system. Lines to guide the eye are included in Fig. 2 and the region with the highest slope is indicated, around the inflection point, where the curve can be approximated as linear.

The three sections in Fig. 2 can be interpreted as domains of different damage formations: (1) damage initiation and the onset of propagation, (2) maximal and constant damage propagation, and (3) onset of damage saturation. In domain 1, damage sites form at energetically favorable positions distributed throughout the sample and start to propagate, mainly perpendicular to the strain direction. In domain 2, there is an equilibrium in damage initiation and crack propagation in combination with stress release and crack arrest through the interaction of neighboring damage sites. Finite element models in the literature show stress concentrations in the substrate at cracked sites in the functional film,[17,18] which leads to strain concentrations and decreased stress in the surrounding regions in the substrate. The stress in the film is at a minimum at cracked sites, with maxima centered between cracks, therefore, an increase in linear crack density counteracts damage propagation. This effect takes over in domain 3, where resistance increase starts to level off.

Identifying the three domains is a very time efficient way of analyzing such datasets. A quick look reveals where domain 2 of damage propagation is present and a goal in developing long-lasting systems would be to shift domain 2 to higher cycle numbers and decrease the slope as much as possible.

In the two studied systems in this work, domain 2 is present at lower cycle numbers (around cycles 150–600) in the Cr–Au system, with a slope of approximately 5×10^{-3} R_0/cycle compared to a slope of approximately 3×10^{-4} R_0/cycle in the region of around cycles 3500 to 9500 in the Au system. The relatively thick Cr interlayer of 30 nm, with a ratio of 1:5 to the 150 nm Au

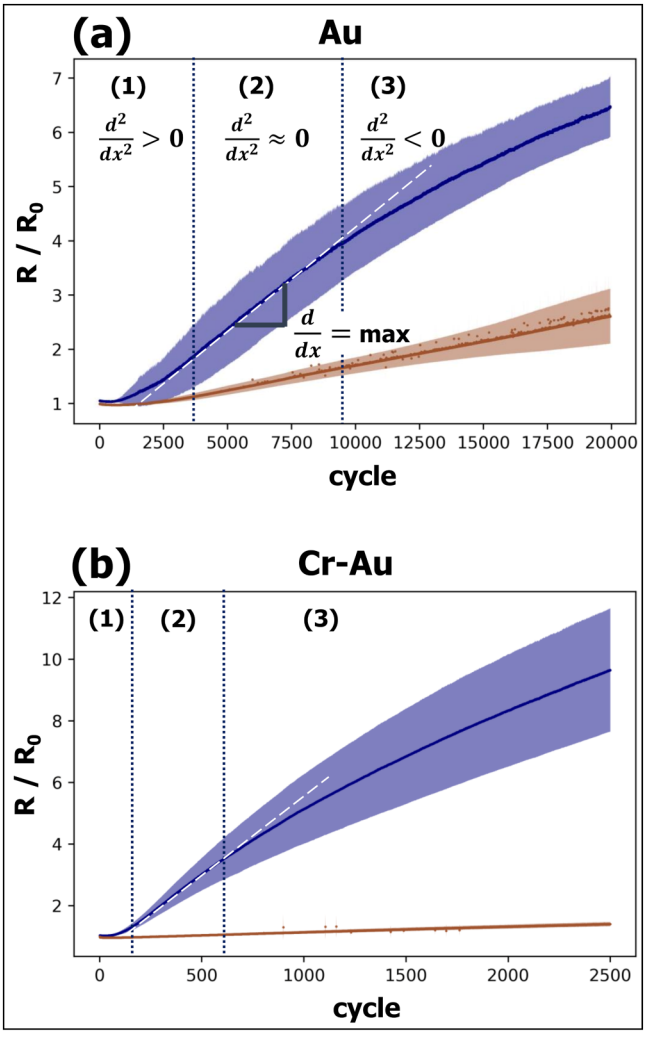

FIG. 2. Maxima and minima resistance values taken during cyclic uniaxial straining to 2% in Au [(a) 20 000 cycles] and Cr–Au [(b) 2500 cycles] of five measurement series—mean ± 1 sample standard deviation. Three damage domains indicate the evolution of maxima values. White dashed lines visualize an approximate linear increase in domain 2. Note: different x- and y-scales.

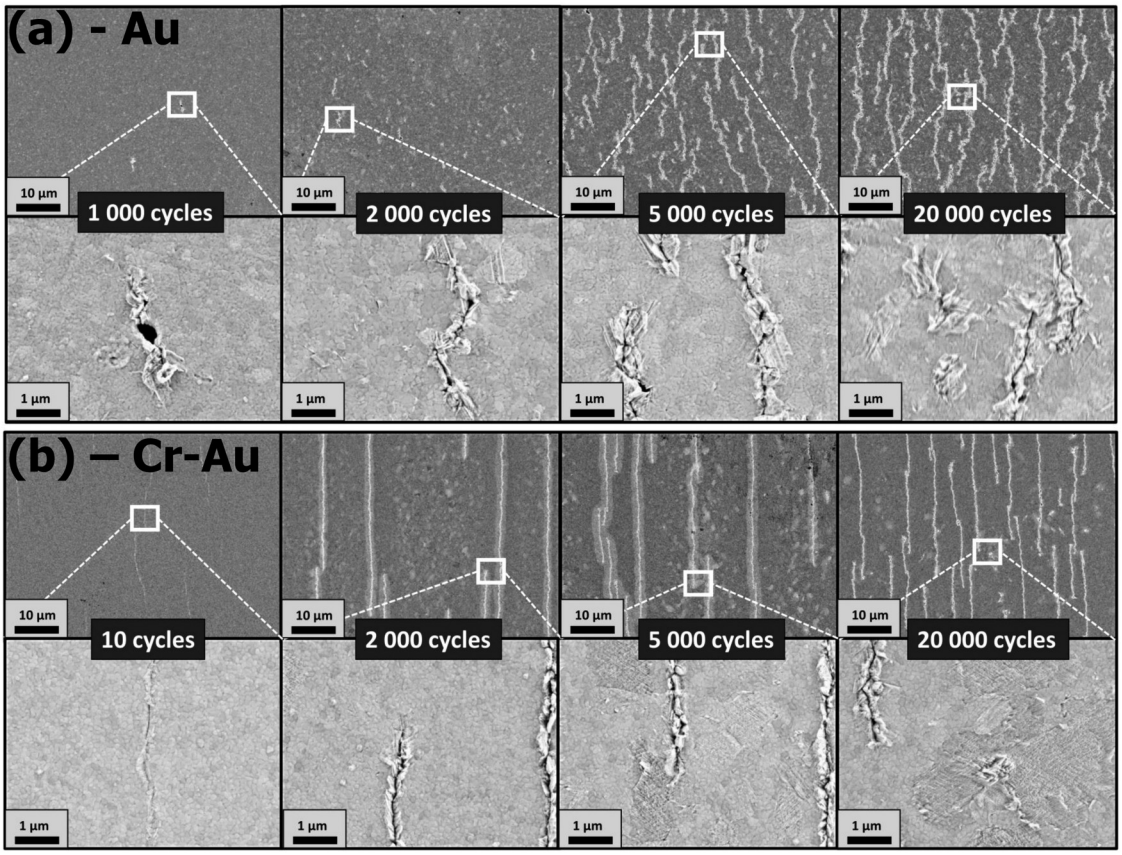

FIG. 3. SEM images of damage evolution for Au (a) and Cr–Au (b), with all images depicting the surface of the Au layer. Lower magnifications are taken with an in-lens secondary electron (SE) detector and higher magnifications with a SE detector at the side of the chamber. Micrographs were taken from different samples and the samples are in the unstrained state.

functional layer leads to faster degradation of the whole system. It is also revealed in SEM images in Fig. 3 that the damage occurs in large parts in domain 2 for both film systems.

A second observation that is apparent from looking at the electrical resistance data is that the resistance amplitude is a lot higher in the Cr–Au system [see Figs. 1(a) and 1(b)]. SEM images (see Fig. 3) show that fewer but longer cracks are present in this system. If the simplified assumption is made that all cracks are fully opened at strain maxima, the conducting pathways running around those cracks could be seen as a network of parallel conductors with a certain resistance at narrow constrictions where cracks meet. A system showing fewer, but longer cracks would consist of less parallel resistances and would show a higher overall resistance than a system with a greater number of parallel resistors of equal magnitude. It is possible that this amplitude is an indication of crack length and the slope in domain 2 could also be an indication, however, more studies are needed to confirm this hypothesis. It is generally known that from one resistance data point, no estimation of crack length can be made, only a product of average crack length and crack density can be determined.[19] However, it could be possible to separate information on those two parameters from an ensemble of data points through the evolution of cycle characteristics. Such datasets contain a variety of additional parameters, such as peak shape and amplitude, and inferred parameters, such as relative and absolute rate of change. Some of those new parameters may show different characteristics for short cracks than they would for long cracks, making it possible to gain information on crack length separately. For example, it was shown that peak widths reflect the formation of through-thickness cracks,[15] and now, it may be the case that this formation occurs slower when shorter cracks are present. However, such correlations are not easily found and require a large number of datasets and thorough analysis.

Previous studies have found abnormally large grain growth during cyclic loading of similar systems[10,20] and the grain size is known to be an important parameter in the fatigue properties of thin metal films. To investigate grain growth, time-intensive methods are necessary, such as EBSD or transmission electron microscopy. However, grain growth will also be reflected in simple electrical resistance measurements. In crystalline metals, electrons scatter at deviations from the periodic potential—this could be

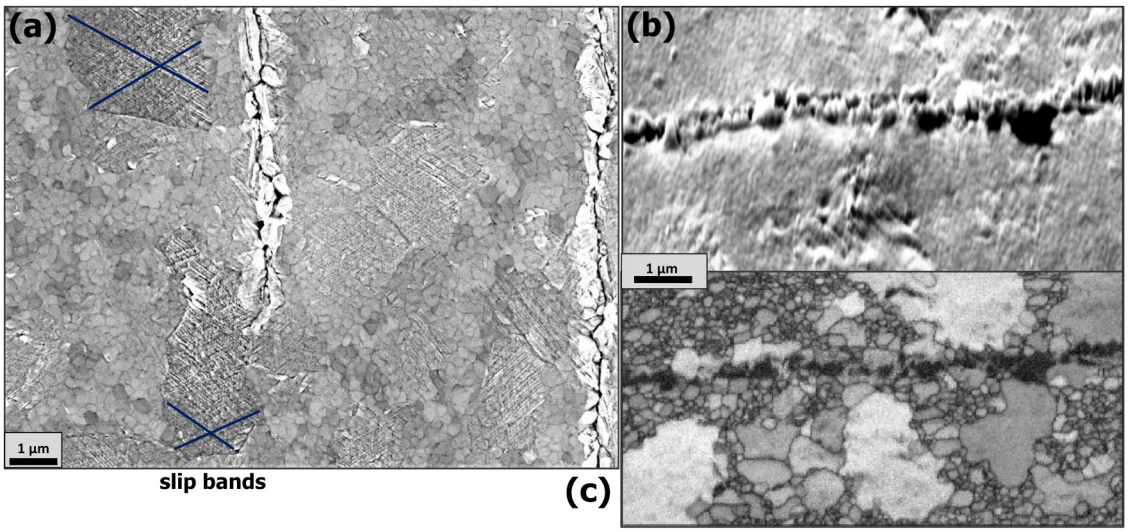

FIG. 4. Slip steps increasing surface roughness and indicating large grains in Cr–Au samples after fatigue loading. (a) Top view SEM image of the Au surface showing slip bands marked by blue lines. (b) SEM overview (70° tilt) of slip steps close to a crack and (c) EBSD band contrast map of the same region depicted in (b), indicating large, singular grains where slip steps are present.

phonons, or defects, such as interstitials and vacancies, impurities, and also grain boundaries. Therefore, the grain size will have an effect on the resistivity of a metal sample.

The samples studied here showed grain growth similar to that observed in the literature.[10,20–22] In in-lens SEM images (lower magnification images in Fig. 3), an increasing number of higher contrast areas can be observed close to cracks and also in areas between cracks. On closer inspection, the lighter areas are roughened surface features due to primary and secondary slip bands and resulting slip steps. An increased surface roughness leads to an increase in secondary electron emission and these surface features appear as bright areas in in-lens images. Figure 4(a) shows a close up of such features with indicated slip bands and Figs. 4(b) and 4(c) show one SEM image with a complementary EBSD band contrast map, showing that those features are actually coarsened grains. The grain growth is also visible in electrical resistance minima values at early cycle numbers, before the resistance increases due to damage propagation are taking over. Figure 5 shows a clear and continuous decrease in electrical resistance at early cycle numbers in the datasets of about 2% in Au and around 4% in Cr–Au. It has to be noted that the largest drop in the very first cycle could be due to a rearrangement of electrical contact with the clamps, but further decrease is most likely occurring due to grain coarsening. An increase in resistance at higher cycle numbers should not be interpreted as an end of grain coarsening, rather than the resistance increase from damage is the primary factor influencing resistance data from there on.

A previous study analyzing the evolution of electrical resistance peak characteristics has shown that full width at half maximum (FWHM) values can reflect the type of damage that is

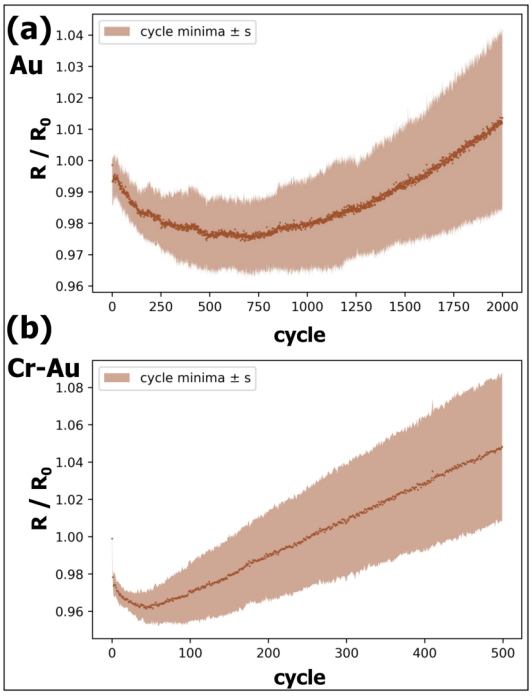

FIG. 5. Initial decrease in minima resistance values for Au (a) and Cr–Au (b), indicating grain growth in the Au layer during early cycling. Mean ± 1 sample standard deviation.

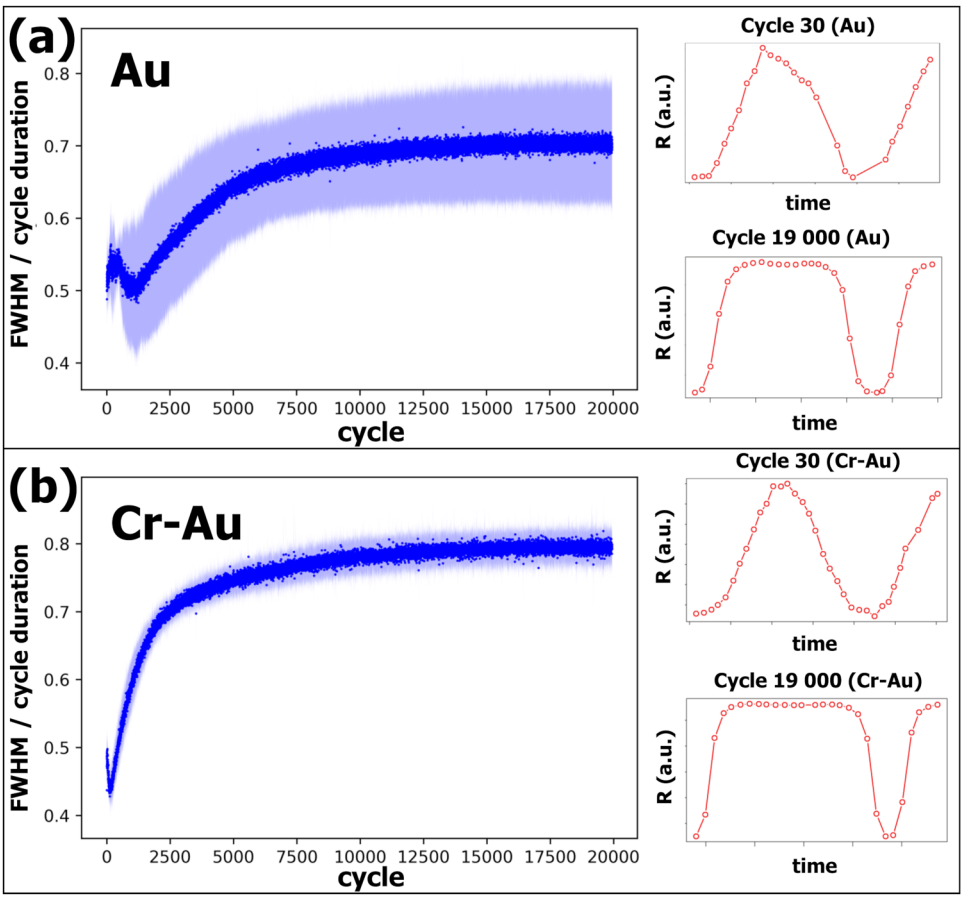

FIG. 6. FWHM values showing a broadening of resistance peaks for both Au (a) and Cr–Au (b)—mean (dark blue) ± 1 sample standard deviation (light blue). Plots of resistance curves for cycle 30 and cycle 19 000 of one measurement series are depicted for each system to visualize the peak broadening.

present to be either surface damage or through-thickness cracks (TTCs).[15] Broad peaks with a plateau around the maximum indicate a complete crack opening before the strain maximum is reached. These broad peaks are a sign that TTCs are present. Narrower peaks, more closely mirroring the applied sinusoidal strain, are an indication of superficial damage and necking of conductive pathways between crack faces during loading. Figure 6 shows the evolution of FWHM values for both investigated systems and for each system one early and one later stage resistance peak is depicted to better visualize this increase in peak width. Two factors influence FWHM values in counteracting ways. Assuming that damage formation and crack propagation within each cycle does not linearly relate to the magnitudes of stresses present in the sample, but happens primarily when stresses are close to their maxima and in term when strain is close to its maximum, pronounced damage formation and propagation within each cycle can lead to sharper peaks and the FWHM value dropping below a value of 0.5 cycle durations, while a high percentage of TTCs present leads to plateaus and an increase in FWHM values. Basically, the sine wave's shape can change to be pointy or flattened, thus changing where the half maximum is located. Both samples show a FWHM value of around 0.5 at the start. This value is expected in undamaged conditions because it is the value that mirrors the sinusoidal applied strain. The drop in FWHM values is present in both systems, but it is more pronounced in the Cr–Au samples at early cycle numbers where significant damage is already introduced after 10 cycles, as can be seen in Fig. 3(b). Both film systems show an increase in peak widths in the scope of the experiment with the increase slowing down at around 6000 cycles for Au, with a FWHM value of around 0.67 cycle durations, and at around 1500 cycles at a value of 0.7 cycle durations for Cr–Au. Here, it can be assumed that the damages present in the systems are mostly TTCs, as was shown in Ref. 15. The values show good reproducibility for the five tested samples each, especially in the Cr–Au system. It has to be noted that this method will not work in an ambient atmosphere for a material, which forms a dielectric oxide layer immediately upon contact with air.

With all data pointing at earlier damage onset, propagation, and saturation in the Cr–Au system, a closer look was taken at the underlying Cr layer in this system. The Au layer was removed with aqua regia which introduces a passivating oxide layer on the Cr interlayer.[23] SEM images in Fig. 7 show the same sample regions before and after the removal of the Au layer after 10 and 1000 loading cycles, with damage sites overlapping in the Cr and Au layer. Linear crack density measurements in the Cr layer showed most of the damage already formed after 50 cycles, with an increase

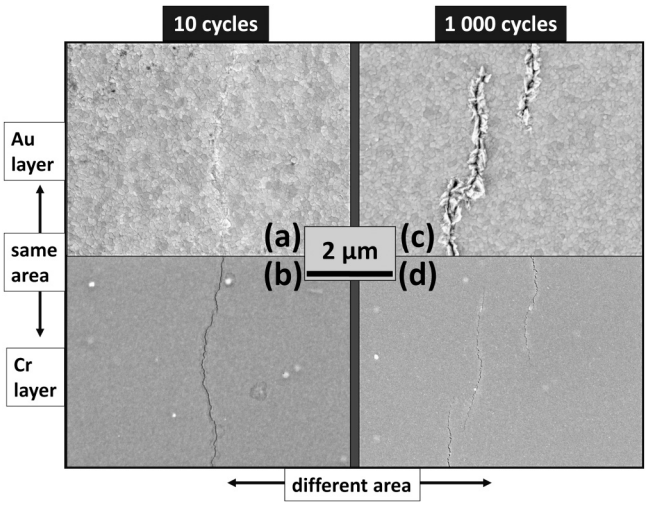

FIG. 7. SEM images of Cr–Au after 10 (a) and (b) and 1000 (c) and (d) cycles to 2% maximum strain. (a) and (c) Au layer. (b) and (d) underlying Cr-layer at the same regions, imaged after chemical removal of Au. Note: the scale bar in the center is valid for all depicted micrographs.

of about 40% from cycle 50 (0.10 ± 0.02 cracks per micrometer) to cycle 1000 (0.14 ± 0.01 cracks/µm). After 10 cycles [Figs. 7(a) and 7(b)], the cracks present in the Cr layer seem to fully permeate the layer's thickness, while the Au layer only shows superficial damage and no through-thickness cracks through both layers are observed. With further cycling to 1000 cycles [Figs. 7(c) and 7(d)], the damage in the Au film propagates in the out-of-plane direction, forming through-thickness cracks. This correlates well with a strong increase in FWHM values in this system [see Fig. 6(b)] and is a good example of the powerful application of one of the methods described in this work.

The presented techniques should be applicable to a wide variety of material systems and cyclic straining experiments. Uniaxial straining was performed in this work, but the methods should also be applicable in the variety of bending tests that have been established in the literature. Acquired electrical resistance datasets from bending experiments can be expected to be similar to those from uniaxial tests since similar types of damage are introduced. Some of the analysis performed in this work requires the samples to be cyclically returned to the unstrained state, which is not the case for sliding-plate tests[24] where different parts of the sample are always under strain. However, resistance data taken in such tests do show similar behavior to the domains of damage formation introduced above.[25] All methods presented can be applicable in other forms of bending test setups where resistance measurements are already performed *in situ*, such as the clap hand test,[26] the two-point rotation test,[27] and outer bending tests.[28] However, in higher frequency experiments, it would be challenging to reach a high enough sampling rate to acquire enough electrical data points per cycle, and the higher data acquisition rate may introduce too much additional noise to analyze single cycle characteristics. One limitation in terms of the material system needs to be emphasized: the method utilizing peak widths is not applicable to materials that quickly form a dielectric oxide layer upon contact with air. The newly formed surfaces from developing through-thickness cracks will not be electrically conductive when they are in mechanical contact at cyclic strain minima.

IV. CONCLUSIONS

It is shown that electrical resistance data taken during cyclic uniaxial loading of thin film conductors contain useful information beyond a simple failure criterion. Electrical data were correlated to three domains of damage propagation and to grain growth. A previously published method for identifying the formation of through-thickness cracks from surface damage through an increase in electrical resistance FWHM values could be verified with congruent SEM images of a Au top layer and a Cr interlayer. A case is made for more extensive use of electrical data, for its ease of acquisition and the possibility of quick and effective *in situ* analysis, once methods of interpreting the data are established.

The presented methods are intended as an expansion of established methods rather than a replacement. Depending on the different intended uses of a functional metal layer, different failure criteria are still absolutely crucial. Lower relative increases of 5% may be used as failure criteria for metallizations carrying higher current densities and in devices where heat dissipation can be a problem, while larger relative increases of up to 100% may be acceptable in transmissions of electrical signals. This work is intended to increase the understanding of failure processes discernible from sets of electrical data to aid in the future development of films and film systems that are able to withstand larger strains and reach their failure criterion only after an increased number of strain cycles. As a next step, more material systems should be examined to verify the applicability of the presented analysis methods.

ACKNOWLEDGMENTS

This work was supported by the Austrian Science Fund (FWF) (Project I, No. 4384-N) and the German Research Foundation (DFG) (No. Grant ME-4368/8) within the framework of the D-A-CH cooperation FATIFACE.

AUTHOR DECLARATIONS

Conflict of Interest

The authors have no conflicts to disclose.

Author Contributions

David D. Gebhart: Conceptualization (lead); Data curation (lead); Formal analysis (lead); Investigation (lead); Methodology (lead); Validation (lead); Visualization (lead); Writing – original draft (lead). **Anna Krapf:** Methodology (equal); Writing – review & editing (equal). **Benoit Merle:** Funding acquisition (equal); Supervision (equal); Validation (equal); Writing – review & editing (equal). **Christoph Gammer:** Supervision (equal); Writing – review & editing (equal). **Megan J. Cordill:** Conceptualization (equal); Funding acquisition (lead); Investigation (equal); Methodology

(equal); Supervision (lead); Validation (lead); Writing – review & editing (lead).

DATA AVAILABILITY

The data that support the findings of this study are available from the corresponding author upon reasonable request.

REFERENCES

[1]G.-D. Sim, Y. Hwangbo, H.-H. Kim, S.-B. Lee, and J. J. Vlassak, Scr. Mater. **66**, 915 (2012).
[2]J. D. Yeager, D. J. Phillips, D. M. Rector, and D. F. Bahr, J. Neurosci. Methods **173**, 279 (2008).
[3]D. Wang, P. A. Gruber, C. A. Volkert, and O. Kraft, Mat. Sci. Eng. A **610**, 33 (2014).
[4]P. Kreiml, M. Rausch, V. L. Terziyska, J. Winkler, and M. J. Cordill, Scr. Mater. **162**, 367 (2019).
[5]N. Lu, X. Wang, Z. Suo, and J. Vlassak, Appl. Phys. Lett. **91**, 221909 (2007).
[6]M. Todeschini, A. Bastos da Silva Fanta, F. Jensen, J. B. Wagner, and A. Han, ACS Appl. Mater. Inter. **9**, 37374 (2017).
[7]M. J. Cordill, O. Glushko, A. Kleinbichler, B. Putz, D. M. Többens, and C. Kirchlechner, Thin Solid Films **644**, 166 (2017).
[8]R. Schwaiger and O. Kraft, Acta Mater. **51**, 195 (2003).
[9]G. P. Zhang, R. Schwaiger, C. A. Volkert, and O. Kraft, Philos. Mag. Lett. **83**, 477 (2003).
[10]H.-L. Chen, X.-M. Luo, D. Wang, P. Schaaf, and G.-P. Zhang, J. Mater. Sci. Technol. **89**, 107 (2021).
[11]M. J. Cordill, T. Jörg, D. M. Többens, and C. Mitterer, Scr. Mater. **202**, 113994 (2021).
[12]X. J. Sun, C. C. Wang, J. Zhang, G. Liu, G. J. Zhang, X. D. Ding, G. P. Zhang, and J. Sun, J. Phys. D: Appl. Phys. **41**, 195404 (2008).
[13]H. Y. Wan, X. M. Luo, X. Li, W. Liu, and G. P. Zhang, Mater. Sci. Eng., A **676**, 421 (2016).
[14]Y.-S. Lee, G.-D. Sim, J.-S. Bae, J.-Y. Kim, and S.-B. Lee, Mater. Lett. **193**, 81 (2017).
[15]D. D. Gebhart, A. Krapf, C. Gammer, B. Merle, and M. J. Cordill, Scr. Mater. **212**, 114550 (2022).
[16]E. Preiß, *Fracture Toughness of Freestanding Metallic Thin Films Studied by Bulge Testing* (FAU University, Erlangen, 2018).
[17]V. M. Marx, F. Toth, A. Wiesinger, J. Berger, C. Kirchlechner, M. J. Cordill, F. D. Fischer, F. G. Rammerstorfer, and G. Dehm, Acta Mater. **89**, 278 (2015).
[18]I. Ben Cheikh, G. Parry, D. Dalmas, R. Estevez, and J. Marthelot, Int. J. Solids Struct. **180-181**, 176 (2019).
[19]O. Glushko, B. Putz, and M. J. Cordill, Thin Solid Films **699**, 137906 (2020).
[20]O. Glushko and M. J. Cordill, Scr. Mater. **130**, 42 (2017).
[21]O. Glushko and M. J. Cordill, JOM **66**, 598 (2014).
[22]O. Glushko and D. Kiener, Acta Mater. **206**, 116599 (2021).
[23]P. Köllensperger, W. Karl, M. Ahmad, W. Pike, and M. Green, J. Micromech. Microeng. **22**, 067001 (2012).
[24]B.-J. Kim *et al.*, Nanotechnology **25**, 125706 (2014).
[25]T.-W. Kim, J.-S. Lee, Y.-C. Kim, Y.-C. Joo, and B.-J. Kim, Materials **12**, 2490 (2019).
[26]S. Kamiya, H. Izumi, T. Sekine, N. Shishido, H. Sugiyama, Y. Haga, T. Minari, M. Koganemaru, and S. Tokito, Thin Solid Films **694**, 137613 (2020).
[27]Q. Guan, J. Laven, P. C. P. Bouten, and G. de With, Thin Solid Films **611**, 107 (2016).
[28]M. Yang, M.-W. Chon, J.-H. Kim, S.-H. Lee, J. Jo, J. Yeo, S. H. Ko, and S.-H. Choa, Microelectron. Reliab. **54**, 2871 (2014).